Evaluation of the Corrosion Barrier Properties of Nano-Reinforced Vinyl Chloride/Vinyl Acetate Coatings

M. Calhoun,[1] A. Ludwick,[1] M. Mahmoud,[2] H. Aglan[1]

[1]*Department of Mechanical Engineering, Tuskegee University, Tuskegee 36088, Alabama*
[2]*Misr University for Science and Technology, Cairo, Egypt*

Received 16 April 2009; accepted 26 May 2009
DOI 10.1002/app.30914
Published online 25 August 2010 in Wiley Online Library (wileyonlinelibrary.com).

ABSTRACT: A poly(vinyl chloride/vinyl acetate) copolymer (VYHH) with and without multiwalled carbon nanotubes (MWCNTs) as reinforcements were used as a coating for steel substrates to evaluate their barrier properties against corrosion. Electrical impedance and thermal properties of the coatings were evaluated. The coatings were formulated with 0.1% MWCNT, by weight. Neat and nano-filled VYHH was used to coat polished, degreased steel substrates via a dipping method. The substrates were either dipped once, for a target coating thickness of 30–40 μm, or twice for a target coating thickness of 60–75 μm. The coated and uncoated control samples were submerged in a tank with a 5% NaCl solution for a 45-day period. Electrochemical impedance spectroscopy (EIS) revealed that coating thickness plays a role in corrosion resistance. EIS also showed that nano-reinforced VYHH had the highest charge transfer resistance within its coating thickness. Fourier transform infrared spectroscopy (FTIR) indicated that hydrolysis occurred in the single coatings for both the neat and nanoreinforced coatings. Differential scanning calorimetry (DSC) and thermo gravimetric analysis (TGA) both showed that the addition of MWCNTs improved the thermal stability of the VYHH. DSC thermograms revealed that the thermal properties of the nano VYHH were largely unchanged after 45 days of submersion as compared with the unaged nano VYHH. © 2010 Wiley Periodicals, Inc. J Appl Polym Sci 119: 15–22, 2011

Key words: VYHH; corrosion; electrochemical impedance; FTIR; DSC; TGA

INTRODUCTION

Nano-filled polymers are a promising alternative to traditional composites for effective barrier protection against degradation due to corrosion. In particular, the addition of multiwalled carbon nanotubes (MWCNTs) in a variety of polymer matrices as reinforcement against corrosion have been studied.[1–3] Defects, cracks and voids are of particular concern in corrosion protection defense as these defects act as pathways that can promote diffusion of the electrolyte through the coating to the substrate. In a well dispersed system, the nanophase is available to fill in defects, nano- to microsized cracks and crevices, thus creating a more cohesive film. By filling the defects, the nanotubes may block existing pathways through the coating thickness, while retarding the advancement of new and partially formed pathways, thus improving the barrier properties of the host polymer to corrosion. A poorly adhered coating will have irregularities and will blister and peel away from the substrate in spots, creating large channels for the electrolyte to contact the substrate.[1,3]

In addition to acting as filler, MWCNTs can improve on the mechanical and thermal properties of a polymer matrix. It has been well documented that MWCNTs have superior properties, such as Young's modulus (≤1 TPa), tensile strength (20–100 GPa), thermal conductivity (6000 W/m/K), high aspect ratio and specific strength (48.5 MN·m/kg), among others. Ganguli et al. studied the effect of loading rate and surface modification of MWCNTs on fracture toughness using a bifunctional epoxy as the polymer matrix. It was found that the addition of 0.15% MWCNTs, by weight, had an 80% improvement on fracture toughness for that system.[4] The addition of carbon nanotubes in a poly(vinyl alcohol) film yielded a 4.5-fold increase in the Young's modulus over neat poly(vinyl alcohol) film.[5] Ryan et al. found that carbon nanotubes promoted crystallinity in the polymer, thus strengthening the matrix. He compared CNTs of different diameters and number of layers, and found that there is a correlation between crystallinity and mechanical performance, regardless of CNT geometries. Carbon nanotubes have also been effectively used as reinforcement against corrosion in electroplated coatings. It was found that the impedance of electrodisposed CNT-

Correspondence to: H. Aglan (aglanh@tuskegee.edu).
Contract grant sponsor: Department of Energy; contract grant number: DE-FG52-05NA27039.

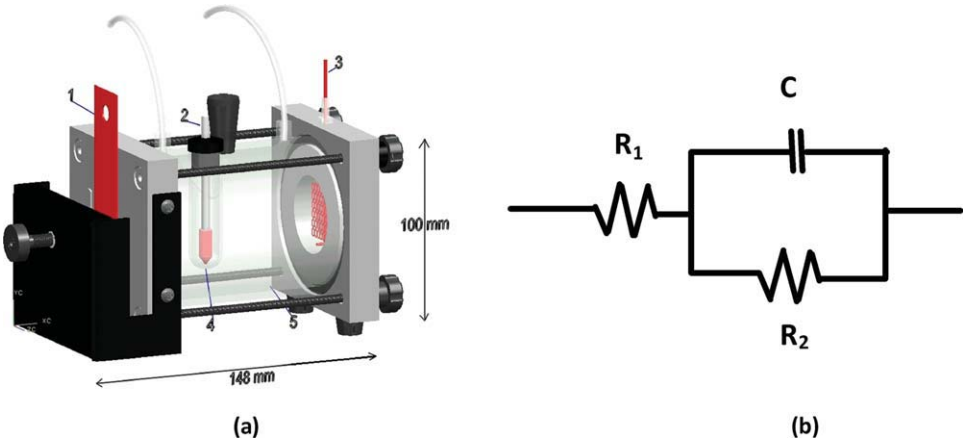

Figure 1 (a) Flat cell and its components, (b) simplified Randles equivalent circuit. [Color figure can be viewed in the online issue which is available at wileyonlinelibrary.com.]

Zn to corrosion was consistently higher than electrodisposed neat Zn coating, indicating that the CNT-Zn coating is more resistant to corrosion.[1]

Electrochemical impedance spectroscopy (EIS) has been used to characterize the corrosion resistance properties in a variety of coatings.[1–3,6–11] EIS takes into account the fact that electrochemical systems can be modeled using electrical circuits. The Randles circuit is a simple representation of an electrochemical system. This is shown in Figure 1(b). In a system where there is a metallic sample with a polymeric coating, the coating separating the metallic substrate and the corrosive electrolyte acts as the dielectric in a double-layered capacitor, denoted by C in the Randles circuit. The resistance of the electrolyte is represented by R_1, and the charge transfer resistance (R_2) represents the resistance of the coating.

Initially, pristine films exhibit high impedances and have a high pore resistance. Pore resistance (R_{pore}) measures the dynamic nature of coatings due to exposure to a corrosive agent over time. The pores in a coating act as transport routes for the electrolyte to penetrate through to the substrate. The pore resistance is also a measure of the porosity and thus is an indicator of degradation. Charge transfer resistance (R_{ct}) measures the amount of diffusion from the metal into an electrolyte after some degradation has occurred to the coating, and the electrolyte has a pathway through the coating to the substrate. The pore resistance is a measure of the coating, whereas charge transfer resistance is descriptive of the metal/coating interface, where the corrosion reaction takes place.[12]

Poly(vinyl chloride-*co*-vinyl acetate) (PVC-*co*-PVAc) is currently used as a protective coating in a variety of applications. PVC-*co*-PVAc has low moisture absorption and thermal expansion. These both are desired attributes of a coating for corrosion protection in that the film will not swell and degrade simply as a result of being in an aqueous environment.[13] Differential scanning calorimetry (DSC) shows that the material is stable up to about 190°C and the amount of crystallinity, or the amount of heat energy required to break the molecular bonds, is highly dependant on the type of solvent used in the formulation.[14] Thermo gravimetric analysis (TGA) on PVC-*co*-PVAc shows a three-stage decomposition profile of weight loss as a function of temperature, with the major decomposition occurring between 250°C and 300°C.[13,15] The addition of MWCNTs to PVC-*co*-PVAcs is expected to improve the thermal properties of the material as thermal properties of CNT/polymer coatings are usually higher than their neat constituents, because of the high thermal characteristic of the CNTs.

In this study, PVC-*co*-PVAc (VYHH) is investigated for effectiveness as a barrier for corrosion protection as a function of both nanoreinforcement and coating thickness. The prepared neat and nano-reinforced specimens were submerged in a 5% NaCl aqueous solution for a period of 45 days. The resistances of the aged samples to corrosion were determined experimentally using EIS and compared with the unaged specimens. Thermal characterization of the neat VYHH and nano VYHH coating was conducted using DSC and TGA. Fourier transform infrared spectroscopy (FTIR) was used to examine the effect of coating thickness on hydrolysis in the system.

MATERIALS AND METHODS

Sample preparation

The VYHH used for this study was provided by Union Carbide and is formulated as an 86 : 14 copolymer, vinyl chloride to vinyl acetate. The polymer was received as a powder and was added at a 23.8% loading, by weight, to a 3.73 : 2.33 : 2.31 mixture of

methyl isobutyl ketone (MIBK), xylene and tolulene, respectively. The mixture was stirred on a magnetic stirrer for at least 24 h, until the VYHH powder was dissolved. The multiwalled carbon nanotubes (MWCNTs) used in this study were provided by Ahwahnee Technologies. The diameter of these tubes is in the range of 2–15 nm, with a length of 1–10 μm, and 5–20 layers. The nanotubes were added to the VYHH at a 0.1% loading rate by weight. In preparation for coating, cold rolled 1010 steel samples (1″ × 4.5″) were cleaned using an equivalent of a grade 0 steel wool and degreased with acetone. Once the substrates were cleaned and the coatings were prepared, the samples were carefully dipped once or twice in either neat VYHH or the nano-reinforced formulation. The target thickness for the single-coated samples was 30–40 μm, whereas the target coating thickness for the double-coated samples was 60–75 μm. The thickness of the polymeric coating was measured using a Time TT260 coating thickness instrument. Care was taken to ensure an even coat over the entire surface of the substrates, particularly over the edges. The samples were left to dry for 3 days. The specimens were then aged for 45 days in a submersion tank with a 5% NaCl solution.

Electrochemical impedance spectroscopy (EIS)

EIS measurements were taken using a potentiostat (Parstat 2273) with a flat cell. The flat cell, pictured in Figure 1(a), shows the sample as the working electrode (1), the reference electrode (2), and the counter electrode (3). The chamber of the cell (5) is filled with an electrolyte solution, thus completing the circuit. The working electrode is affixed to the cell with a screw and is exposed to the solution in a 1 cm^2 area. Figure 1(b) depicts a simplified Randles ciruit that was used as an equivalent circuit for the samples exhibiting a low-pore resistance. In this scheme, the testing was conducted over a frequency range of 1×10^6 Hz to 1×10^{-2} Hz with 10-mV amplitude.

Fourier transform infrared spectroscopy

FTIR spectra for both the aged and unaged materials were captured using a Nicolet 6700 FTIR spectrometer with an attenuated total reflectance (ATR) accessory. The FTIR spectrometer has a spectral resolution of 4 cm^{-1} over a 4000 – 400 cm^{-1} range in absorbance mode. Each sample was scanned a total of 32 times.

Thermal analysis

TGA was performed using a 2050 Thermo gravimetric analyzer manufactured by TA Instruments. The experiments were conducted under air at a temperature range of 30°C–600°C ramping at 10°C/min. Weight loss as a percentage of total initial weight and the derivative weight loss curves as a function of time are reported. DSC was performed using a DSC Q1000 manufactured by TA Instruments. The experiments were performed using a temperature range from 30°C to 300°C at 10°C/min under nitrogen. Specimens for TGA and DSC measurements were cut from the peeled film before and after 45 of submersion. The DSC specimens were between 5 and 10 mg, and the TGA specimens were 30–40 mg, by weight.

RESULTS AND DISCUSSION

EIS measurements

EIS was performed on bare steel as well as neat VYHH (V) and VYHH with 0.1% MWCNTs (VN) for single- and double-coated samples before submersion, at 7 and 45 days. Five specimens were tested for each formulation. Representative spectra are shown in Figures 2–5. All |z| values discussed were measured at the low end of the frequency range, at 0.01 Hz, for ranking purposes. Figures 2 and 3 show the impedance and phase angles plotted against frequency for the single-coated neat and MWCNT reinforced VYHH, respectively. It can be seen from the figures that the coating resistance for the single-coated specimens decreased as a function of time with exposure to the salt solution. Initially, the R_{pore} for the single-coated samples was on the order of 10^9 Ω cm^2. By day 45, the R_{ct} was apparent and dominant and was on the order of 10^5 Ω cm^2 for both the single-coated neat and the nanoreinforced VYHH samples. It is evident that diffusion of the electrolyte to the substrate occurred in both the neat and nanoreinforced single-coated samples after

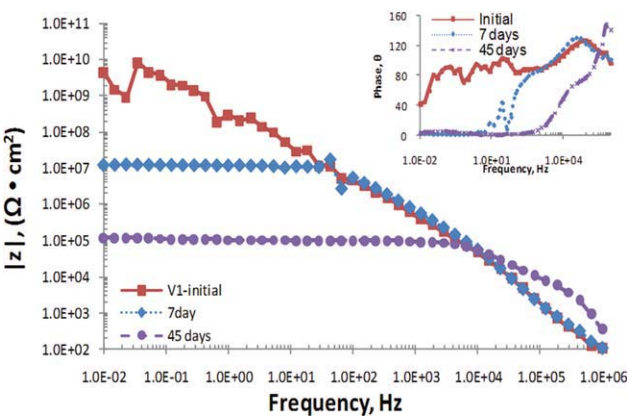

Figure 2 Bode plot for impedance with phase plot inset for single-coated neat VYHH (V1) over a 45-day period. [Color figure can be viewed in the online issue which is available at wileyonlinelibrary.com.]

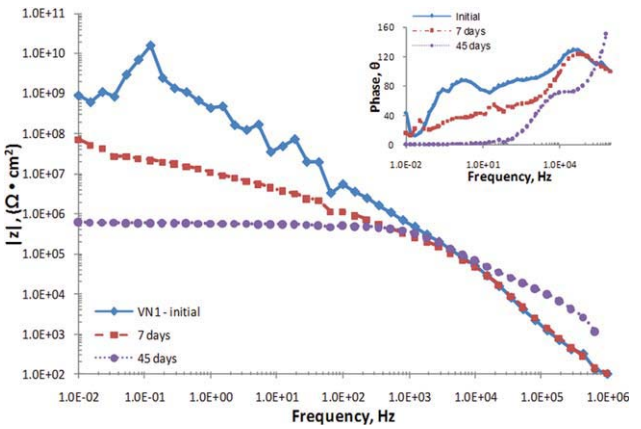

Figure 3 Bode plot for impedance with phase plot inset for single VYHH/ MWCNT (VN1) coating over a 45-day period. [Color figure can be viewed in the online issue which is available at wileyonlinelibrary.com.]

45 days. Visually, blisters were observed in the single-coated samples after only 7 days. By day 45, discoloration due to the corrosion of the steel could be seen on both the neat and nano coatings. The phase diagrams for the aged specimen show the phase angle at the lower frequencies to be near zero, indicating a resistive behavior at those frequencies. In the V1 (single-coated neat VYHH) samples, the phase angle is small at frequencies 9 Hz and lower by day 7 and at all frequencies 500 Hz and smaller by day 45. The positive phase angle at the higher frequencies indicates that the coating is exhibiting inductive behavior. With time, the reactants in the electrolyte increase the porosity of the coating, eventually accelerating the degradation of the coating.

Figures 4 and 5 show the impedance and phase angles with frequency for V2 and VN2 specimens. Again, both coatings exhibit high initial R_{pore} values, as evidenced by a near −1 upward slope through the entire frequency range. The R_{pore} observed are seen in the order of 10^9 Ω·cm^2. By day 45, the observed R_{ct} for both specimens is still high, with the VN2 specimen maintaining virtually no loss in impedance over 45 days (R_{ct} on the order of 10^9 Ω·cm^2), whereas the impedance of the V2 specimen decreased by one order of magnitude. The higher impedance of the nano-reinforced VYHH coating after 45 days indicates that there is some advantage in using nano-reinforcement for improvement in barrier protection. This result is in agreement with the single-coated samples, though the values are substantially higher. The double-coatedsamples have R_{ct}s that are at least five orders of magnitude higher than the single-coated samples after 45 days of aging. The impedance for coated and uncoated neat and nano-VYHH before and after submersion is summarized in Table I.

It is well known that there is a correlation between coating thickness and impedance. However, the addition of a nanophase in an organic coating may yield some opportunity to use a thinner coating, because it is believed that nanoparticles can fill the surface irregularities on the surface of the substrate, improving the wetting of the substrate and thus improving the barrier protection properties while using less material. The average coating thickness for the double-coated films is 76.3 ± 19.7 μm, while the one-coat film's average thickness is 27.3 ± 6.6 μm. Within each coating thickness, the nano-reinforced coatings exhibited a higher R_{ct} than the neat VYHH within their coating thicknesses. Apparently, the addition of MWCNTs improved the barrier properties of the coatings by increasing the interfacial adhesion between the coating and the substrate. It seems that the MWCNT reinforced coating has more capability to fill crevices on the surface of the steel substrate than the unfilled coating. The fact that the nano-reinforced samples (VN) consistently had higher impedances within their coating

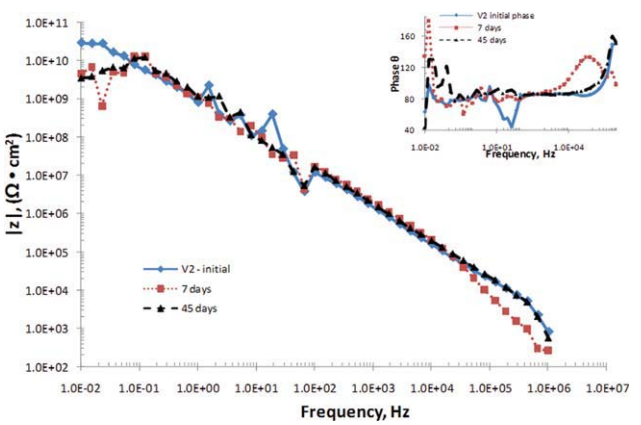

Figure 4 Bode plot for impedance with phase plot inset for double neat VYHH (V2) coating over a 45-day period. [Color figure can be viewed in the online issue which is available at wileyonlinelibrary.com.]

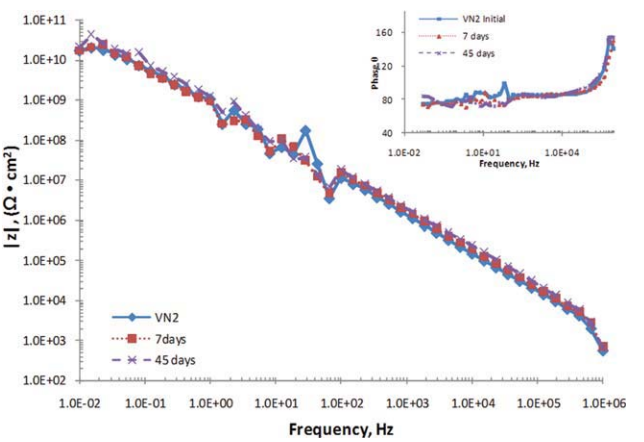

Figure 5 Bode plot for impedance with phase plot inset for double VYHH/MWCNT (VN2) coating over a 45-day period. [Color figure can be viewed in the online issue which is available at wileyonlinelibrary.com.]

thickness relative to the neat samples (V) over time indicates that overall, the nano-reinforced coatings display a higher resistance to corrosion. Visually, the single-coated specimens had the most obvious signs of corrosion after exposure. This was apparent after just 7 days, particularly in the neat coating. The VN2 coating overall showed the least amount of wear due to corrosion.

FTIR analysis

Figure 6 shows FTIR spectra for single- and double-coated neat and nano-reinforced VYHH films after 45 days of submersion. The aged single-coated neat and MWCNT reinforced VYHH samples show a very broad absorption from 3000 cm^{-1} to 3500 cm^{-1}. These broad absorptions in the thin film are the resultant of both symmetric and asymmetric stretching vibrations of water molecules indicating significant water absorption by the coating, contributing to the hydrolysis of the acetate pendant of the VYHH polymer during the aging period.[16] The intensity of this broad band is most prominent in the neat VYHH single-coated sample. The peak appearing at 2925 cm^{-1} is assigned to the C—H stretch along the molecular chain backbone. The intensity of this peak seems to diminish slightly with the appearance of the broad band attributed to water molecules. The peak at 1737 cm^{-1} is assigned to the C=O stretch in the unhydrolyzed ester group.[17] This peak is most intense for the double-coated neat and nano-reinforced samples, as indicated by the enlarged segment of the spectra at 1737 cm^{-1} displayed in Figure 6. Thicker coatings provide longer pathways to the substrate, which may significantly slow the permeation of the electrolyte through the coating. One the other hand, nano-reinforcements can fill voids and defects, thus reducing the number of pathways through the coating, thus retarding the effect of hydrolysis. The advantages of both coating thickness and the presence of a nanophase are evidenced by FTIR spectra.

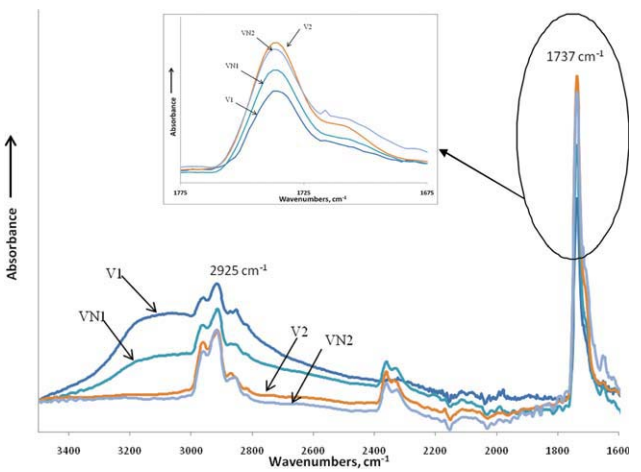

Figure 6 FTIR spectra for V1, VN1, V2, and VN2 specimens after 45 days of submersion. [Color figure can be viewed in the online issue which is available at wileyonlinelibrary.com.]

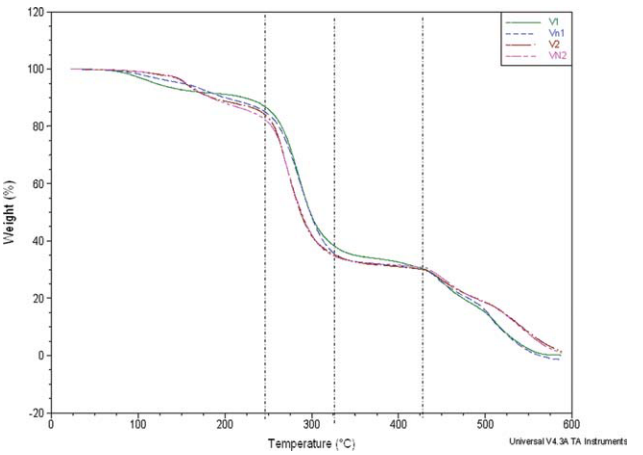

Figure 7 TGA thermogram for unaged single- and double-coated neat and MWCNT-reinforced VYHH run in air. [Color figure can be viewed in the online issue which is available at wileyonlinelibrary.com.]

Thermogravimetric analysis (TGA)

The thermograms for single- and double-coated neat and nano-reinforced VYHH before and after immersion are shown in Figures 7 and 8, respectively. As can be seen in the thermograms, the decomposition curves are very similar for the unaged samples (Fig. 7). There is an initial decrease seen in all of the samples to 80–85% of initial weight by 250°C, indicating loss of free and bound water in the coatings that

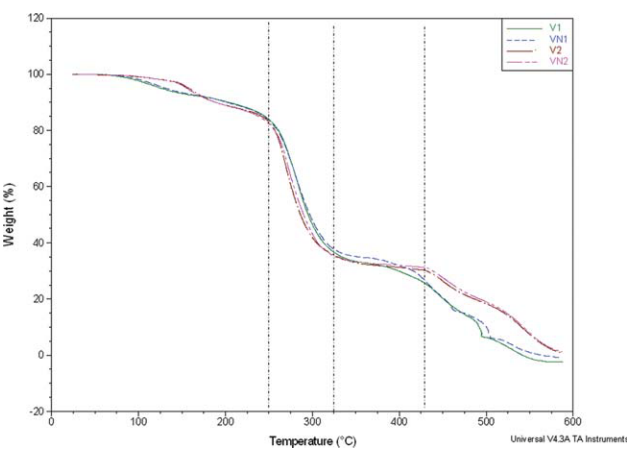

Figure 8 TGA thermogram for single- and double-coated neat and MWCNT-reinforced VYHH submerged for 45 days, run in air. [Color figure can be viewed in the online issue which is available at wileyonlinelibrary.com.]

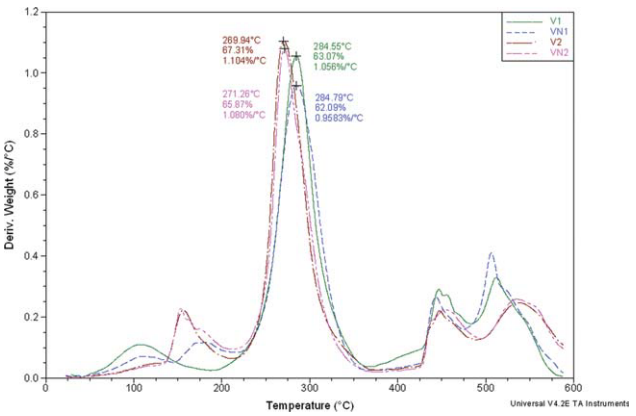

Figure 9 Derivative TGA thermogram for V1, VN1, V2, and VN2 specimen submerged for 45 days. [Color figure can be viewed in the online issue which is available at wileyonlinelibrary.com.]

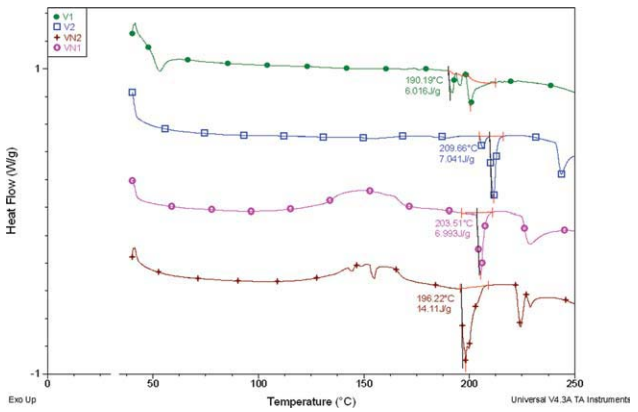

Figure 10 DSC thermogram for unaged single- and double-coated neat and nano-reinforced VYHH. [Color figure can be viewed in the online issue which is available at wileyonlinelibrary.com.]

were present past post cure of the material. After 250°C, a sharp decrease in weight is seen in all of the unaged single- and double-coated samples. At 330°C, the samples have lost 60–65% of their original weight. The decomposition of PVC-*co*-PVAc typically occurs as a result of the acetate and chloride pendants groups breaking away from the backbone of the molecular chain, giving off volatile HCl and acetic acid.[15] A final weight loss stage is seen after 430°C, and 100% decomposition occurs after 600°C. This three stage thermal decomposition pattern is typical for PVC-co-PVAcs.[13,15] A similar trend was seen with the aged coatings (Fig. 8), with maxima again appearing at 250°C and 330°C. Derivative thermograms for the aged neat and nano-reinforced single- and double-coated samples are given in Figure 9. Two replicates were performed for each coating. The peak seen after 100°C indicates the loss of water, which was absorbed during submersion. The peaks are larger for the single-coated specimens, V1 and VN1, than the double-coated specimens, V2 and VN2. The peaks for the single-coated specimens are observed to be broad, spanning from roughly 50°C to 130°C. This suggests that there was both bound and unbound water in the specimens. This agrees with the FTIR spectral data.

Also, it was observed that the peak derivative weight change is lower for the nano-reinforced coatings than the neat coatings. They were measured to be 0.96 ± 0.06%/°C for theVN1 specimens and 1.06 ± 0.01%/°C for the V1 specimens. The double-coated specimens' peak derivative weight change was found to be 1.08 ± 0.03%/°C and 1.10 ± 0.06%/°C for the VN2 and V2 specimens, respectively. These results indicate that the nano-reinforced coatings are more thermally stable than their neat formulations after submersion. This was more apparent in the single coatings than the double coatings.

Differential scanning caloriemetry

DSC thermograms of single- and double-coated neat and nano-reinforced VYHH are given in Figures 10 and 11 for unaged and aged samples, respectively. A minimum of two scans were performed for each coating. Representative thermograms are shown. Endotherms due to crystalline melting are seen between 175°C and 210°C in both the aged and unaged samples (Figs. 10 and 11). DSC scans were run for the neat VYHH powder, however, there was no crystalline melting endotherm seen in those scans, indicating that the crystallinity was induced by the solvents in the system evaporating at low temperatures.[13] From Figure 10, it is seen that the enthalpies for the unaged V1, V2, VN1 and VN2 samples are 6.02, 7.04, 6.99, and 14.11 J/g, respectively. The samples containing nano-reinforcements required the most energy to complete the endothermic transition within their coating thickness. MWCNTs used in polymer systems will often act as

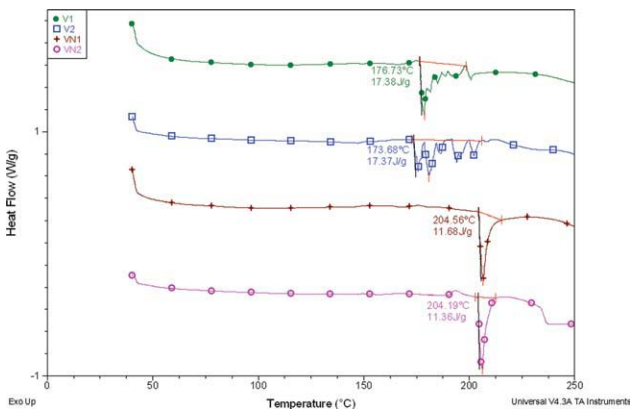

Figure 11 DSC thermogram for single- and double-coated neat and nano-reinforced VYHH after 45 days of aging. [Color figure can be viewed in the online issue which is available at wileyonlinelibrary.com.]

TABLE I
Impedances for Coated and Uncoated Neat and Nano VYHH Before and After Submersion

		$R_{ct.}$ Submerged $\Omega \cdot cm^2$	
Samples	R_p, Initial	After 7 days	After 45 days
Bare steel	1.11×10^3	–	–
V1	83.1×10^8	12.2×10^6	115×10^3
VN1	16.4×10^9	72.5×10^6	655×10^3
V2	28.5×10^9	13.6×10^9	34.7×10^8
VN2	20.9×10^9	24.6×10^9	19.1×10^9

nucleation sites and to increase the percentage of crystallinity in polymer systems.[18,19] The double-coated nano-reinforced coating had the highest crystalline melt enthalpy, more than twice that of any of the other coatings, which suggests that there were more nucleation sites for crystallization to occur because the thicker coating created a more cohesive film with fewer defects than the single-coated films. The single-coated films had the lowest enthalpies, regardless as to whether or not nano-reinforcements were used. There was a difference of <1 J/g between the enthalpies of the single-coated neat and nanofilms. Nevertheless, it should be noted that these crystalline melt energies are quite small, and this system is largely amorphous.

After aging, the endotherms seen in the neat single and double VYHH coatings occurred on average 25°C lower than those seen in the thermograms of the unaged material, at 176.73°C and 173.68°C aged versus 190.19°C and 209.66°C unaged, for the single- and double-coated VYHH, respectively. In addition, the endotherms for the aged VYHH materials are very broad with several small peaks. The enthalpies for the aged coatings are 17.38, 17.37, 11.68, and 11.36 J/g for the V1, V2, VN1, and VN2 coatings, respectively. After aging, it is seen that the neat VYHH required much more energy to complete crystallization melt than the unaged neat VYHH. During exposure, the NaCl solution diffused through the coatings whereby molecules in the NaCl solution were able to freely interact with the VYHH molecule chains, causing relaxation in the chains. Because of this relaxation in the molecular chains, the crystalline melt temperature decreased, but because these interaction sites are random, crystalline melting occurred over a wider temperature range, and required more energy to complete the transition than the unaged coatings.

The endotherms for the aged single- and double-coated nano-reinforced VYHH can be seen at 204.56°C and 204.19°C versus 203.51°C and 196.22°C for the unaged single- and double-coated nano-reinforced VYHH, respectively (Fig. 11). The peak crystalline melt temperature as a function of aging is mostly unaffected by addition of MWCNTs. The melt peaks for the aged nano-reinforced coatings are deep and narrow, which indicate that the molecular chains in the crystalline portion of the nano coatings did not relax as was seen in the neat VYHH coatings. There was a decrease seen in the enthalpy of the aged double nano coatings from 14.11 to 11.36 J/g. This result is expected and is corroborated with EIS data for the peeled nano-coated steel indicating that there was some loss in R_{ct} with exposure. To a lesser extent, differences seen in enthalpies may also be a function of the randomness of the distribution and number of nucleation sites at the MWCNTs. Because both peak crystalline melt temperature and total crystalline melt enthalpy of the nano coatings were largely unchanged as a result of exposure, the introduction of MWCNTs in VYHH creates a coating with better barrier properties than neat VYHH; a more cohesive coating, with better barrier properties against corrosion.

CONCLUSIONS

Neat and nano VYHH coatings on steel substrates were prepared and submerged in a 5% NaCl solution for a period of 45 days.

- The nano-reinforcement in the VYHH improved the barrier properties against corrosion over the neat VYHH throughout the 45-day duration of the experiment within each coating thickness. The impedances of the single coatings are lower than that of the double coatings, which affirms the correlation between coating thickness and corrosion resistance.
- FTIR analysis showed hydrolysis occurred in both the neat and nano single VYHH coatings. The amount of hydrolysis was less than that of neat with the addition of the nanophase. This indicates that both coating thickness and the presence of a nano-reinforcement play a role in corrosion protection. This result is in agreement with the EIS data.
- TGA thermograms show that overall, the decomposition profiles of the neat and nano VYHH are very similar, however, the nano VYHH coatings have a slower peak decomposition rate than the neat VYHH within each coating thickness.
- Weight loss related to hydrolysis was clearly seen in the derivative TGA thermogram. The weight loss peak was more pronounced in the single-coated specimens than the double-coated specimens. This finding correlates with the FTIR spectral data.
- DSC thermograms revealed that the peak melt temperature of the neat VYHH decreased by an average of 25°C after aging and the transition

occurred over a broad temperature range. There was no change in the peak melt temperature in the nano coatings, and crystalline melting occurred over a very narrow temperature range. Molecular chain relaxation occurred in the neat VYHH, causing the downward shift in melt temperature, whereas there was no evidence of chain relaxation in the nano-reinforced coatings. It is believed that chain relaxation is a result of diffusion of the NaCl solution through pathways in the film, and that the nanophase restricts the interaction between Na^+ and the polymer chains.

The authors acknowledged Lazborne Allie and Adam Charlton for their assistance with sample preparation and EIS testing.

References

1. Praveen, B. M.;Venkatesha, T. V.; Naik, Y. A.; Prashantha, K. Surf Coat Technol 2007, 201, 5836.
2. Chen, X. H.; Chen, C. S.; Xiao, H. N.; Cheng, F. Q.; Zhang, G.; Yi, G. J. Surf Coat Technol 2005, 191, 351.
3. Aglan, A.; Allie, A.; Ludwick, A.; Koons, L. Surf Coat Technol 2007, 202, 370.
4. Ganguli, S.; Aglan, H.; Dennig, P.; Irvin, G. J Rein Plast Comp 2006, 25, 175.
5. Ryan, K. P.; Cadek, M.; Nicolosi, V.; Blond, D.; Ruether, M.; Armstrong, G.; Swan, H.; Fonesca, A.; Nagy, J. B.; Maser, W. K.; Blau, W. J.; Coleman, J. N. Comp Sci Tech 2007, 67, 1640.
6. Lendvay-Gyorik, G.; Pajkossy, T.; Lengyel, B. Prog Org Coat 2006, 56, 304.
7. Yang, L. H.; Liu, F. C.; Han, E. H. Prog Org Coat 2005, 53, 91.
8. Fang, J.; Xu, K.; Zhu, L.; Zhou, Z.; Tang, H. Corros Sci 2007, 49, 4232.
9. Gonzalez-Garcia, Y.; Gonzalez, S.; Souto, R. M. Corros Sci 2007, 49, 3514.
10. Hur, E.; Bereket, G.; Sahin, Y. Curr Appl Phy 2007, 7, 597.
11. Mansour, E. M. E.; Abdel-Gaber, A. M.; Abd-El Nabey, B. A.; Tadros, A.; Aglan, H.; Ludwick, A. Corrosion 2002, 58, 113.
12. Loveday, D.; Peterson, P.; Rodgers, B. JCT Coat Tech 2004, 1, 88.
13. Chattopadhyay, S.; Madras, G. Polym Degrad Stab 2002, 78, 519.
14. Das, G.; Banerjee, A. N. Eur Polym J 1995, 8, 973.
15. Galikova, A.; Subrt, J.; Bastl, Z.; Kupcik, J.; Blazevska-Gilev, J.; Pola, J. Thermo Acta 2006, 447, 75.
16. Ohman, M.; Persson, D. Electrochim Acta 2007, 52, 5159.
17. Peprnicek, T.; Kalendova, A.; Pavlova, E.; Simonik, J.; Duchet, J.; Gerard, J. F. Polym Degrad Stab 2006, 91, 3322.
18. Kanagaraj, S.; Varanda, F. R.; Zhil'tsova, T. V.; Oliveira, M. A. S.; Simões, J. A. O. Comp Sci Tech 2007, 67, 3071.
19. Ryan, K. P.; Cadek, M.; Nicolosi, V.; Walker, S.; Ruether, M.; Fonseca, A.; Nagy, J. B.; Blau, W. J.; Coleman, J. N. Synth Met 2006, 56, 332.